Lidar vertical observation network and data assimilation reveal key processes driving the 3-D dynamic evolution of $PM_{2.5}$ concentrations over the North China Plain

Yan Xiang[1], Tianshu Zhang[2, 1], Chaoqun Ma[3], Lihui Lv[1], Jianguo Liu[2], Wenqing Liu[2, 1], and Yafang Cheng[3]

[1]Institutes of Physical Science and Information Technology, Anhui University, Hefei 230601, China
[2]Key Laboratory of Environmental Optics and Technology, Anhui Institute of Optics and Fine Mechanics, Chinese Academy of Sciences, Hefei 230031, China
[3]Minerva Research Group, Max Planck Institute for Chemistry, Mainz, Germany

Correspondence: Yan Xiang (yxiang@ahu.edu.cn) and Yafang Cheng (yafang.cheng@mpic.de)

Abstract: China has made great efforts to monitor and control air pollution in the past decade. Comprehensive characterization and understanding of pollutants in three-dimension (3-D) are, however, still lacking. Here, we used data from an observation network consisting of 13 aerosol lidars and more than 1000 ground observation stations, combined with a data assimilation technique, to conduct a comprehensive analysis of an extreme heavy aerosol pollution (HAP) over the North China Plain (NCP) from November–December 2017. During the studied period, the maximum hourly mass concentration of surface $PM_{2.5}$ reached ~390 $\mu g \cdot m^{-3}$. After assimilation, the correlation between model results and the independent observation sub-dataset was ~50% higher than the that without the assimilation, and the root mean square error was reduced by ~40%. From pollution development to dissipation, we divided the HAP in the NCP (especially in Beijing) into four phases—an early phase (EP), a transport phase (TP), an accumulation phase (AP), and a removal phase (RP). We then analyzed the evolutionary characteristics of $PM_{2.5}$ concentration during different phases on the surface and in 3-D space. We found that the particles were mainly transported from south to north at a height of 1-2 km (during EP and RP) and near the surface (during TP and AP). The amounts of $PM_{2.5}$ advected into Beijing with the maximum transport flux intensity (TFI) were through the pathways in the relative order of the southwest > southeast > east pathways. The dissipation of $PM_{2.5}$ in the RP stage (with negative TFI) was mainly from north to south, with an average transport height of ~1 km above the surface. Our results quantified the multi-dimensional distribution and evolution of $PM_{2.5}$ concentration over the NCP, which may help policymakers develop efficient air pollution control strategies.

1 Introduction

Frequent heavy air pollution has exerted significant impacts on air visibility, climate, human health, and other environmental concerns (Gao, Woodward, et al. 2017; Pokharel et al. 2019; Su, Cheng, and Poschl 2020). As a developing country with the largest population in the world, China's air quality has exhibited an obvious improvement trend in recent years (Zhang and Cao 2015; Cao et al. 2017). Regional air pollution in China is still serious, however, especially the heavy aerosol pollution (HAP) caused by fine particulate matter ($PM_{2.5}$) in winter, which has attracted attention worldwide (Zheng et al. 2019; Li, Zhang, et al. 2017; Zheng et al. 2015; Cheng et al. 2016). Therefore, providing a reliable distribution of the $PM_{2.5}$ concentration of HAP, especially at any time and at any height in a given region, is particularly important in the quest of the public to avoid health problems and to provide government policy makers with help in designing effective controls (Hu et al. 2015).

Compared with other air pollutants (e.g., ozone and nitrogen dioxide), $PM_{2.5}$ has a longer atmospheric lifetime (3–5 days), during which it can be transported vertically to great heights and horizontally hundreds of kilometers (Wang et al. 2017; Zhang et al. 2014), depending on the meteorological conditions (e.g., relative humidity and precipitation) and chemical composition (Yang et al. 2017). Previous study demonstrated that regional transport plays an important role for pollution formation in major cities of China, e.g., transport contributes over 50% of the $PM_{2.5}$ mass concentration in Beijing city, Shanghai city, Hangzhou city, Guangzhou city, Hong Kong and Chengdu city during the relatively polluted period (Sun et al. 2017). From 2005–2010, annually, about 35.5% (32.8 $\mu g \cdot m^{-3}$) of the $PM_{2.5}$ in Beijing was attributed to regional transport from the North China Plain (NCP), within which up to 60.4% (64.3 $\mu g \cdot m^{-3}$) from southerly and westerly air flows (Wang et al. 2015). Since the 2013 implementation of the most stringent clean air policy in China, the control of local pollution sources has led to the rapid reduction of total $PM_{2.5}$ concentration (Zhang, Zheng, et al. 2019). It should be noted, however, that the local contributions, intra-regional transport, and inter-regional transport accounted for 47% (12.7 $\mu g \cdot m^{-3}$), 25% (6.6 $\mu g \cdot m^{-3}$), and 28% (7.6 $\mu g \cdot m^{-3}$), respectively, of the total $PM_{2.5}$ for the Beijing-Tianjin-Hebei (BTH) region from 2014–2017, with the 2017 contribution of regional transport to the BTH concentration rate ranging from 32.5–68.4% (Dong et al. 2020).

Previous studies have shown that it is difficult to use surface observations to characterize the impact of upper-level pollutants in the atmosphere (Huang, Wang, and Ding 2018), which is affected by local emissions, regional transport, meteorological conditions, geographical

factors etc. (Tao et al. 2020; Che, Gui, et al. 2019). Therefore, understanding the key processes that drive the dynamic temporal and spatial evolutionary characteristics of pollutants on the NCP is essential for revealing the source and transport of aerosols, which has different radiative forcing at different heights (Kumar et al. 2017; Che, Xia, et al. 2019). Actually, stereo-monitoring devices and technologies, such as lidar (Sheng et al. 2019; Fan et al. 2019; Chen, Schofield, et al. 2019), MAX-DOAS (Hong et al. 2018; Zhang et al. 2020), and satellite remote sensing (Pang et al. 2018; Schwartz et al. 2012; Zhang, Liu, et al. 2019), can reveal the vertical distribution of pollutants at different heights (Tian et al. 2017; Heese et al. 2017). Due to the limited spatial and temporal observations, however, it is impossible to provide physical and chemical properties in the atmosphere at any time period and on any path, which makes it difficult to directly reveal the formation and source of pollution.

On the other hand, although the distribution of pollutants can be simulated by air quality models (Huang et al. 2018; Zhang et al. 2008), large uncertainties remain, mainly from the influence of emission inventory, meteorological fields, and some hypothetical conditions (Xu et al. 2016; Chen et al. 2017; Huang et al. 2016). Fortunately, the above observed data and the results of the model can be fused using data assimilation techniques, which can correct the model simulation results via the observed data (Wang et al. 2013; Ma et al. 2019). Research has shown that mainstream data assimilation (DA) technologies, including 3DVAR (Jiang et al. 2013; Ma et al. 2018), 4DVAR (Yumimoto et al. 2008), and EnKF (Chen, Liu, et al. 2019), can be used to assimilate observation data from the surface, remote sensing data (such as AOD) from satellites, and vertical profile data from lidar, all of which can be used to improve the performance of the model, including the simulation of $PM_{2.5}$ and PM_{10}.

In this study, we analyzed the observation data from a vertical observation network consisting of 13 lidars and surface observation stations during an extreme pollution event in eastern China, especially in the NCP. Next, all of the data were utilized by the Gridpoint Statistical Interpolation (GSI) three-dimensional (3-D) variational (3DVAR) data assimilation system to revise the $PM_{2.5}$ results from the WRF-Chem simulation (Pagowski et al. 2014). Finally, the multi-dimensional evolutionary characteristics of $PM_{2.5}$ at the surface and in the vertical layer, as well as the 3-D distribution, were analyzed in detail. Although data assimilation has been applied in China using surface observation network data (Gao, Saide, et al. 2017), AOD (Saide et al. 2014; Saide et al. 2013; Schwartz et al. 2012; Liu et al. 2011), and lidar data (Cheng et al. 2019), to our knowledge, this is the first attempt in China to apply lidar network data to assimilation technology, from which the high-precision 3-D distribution of

pollutants can be provided, thus supplying effective data support for clarifying the formation mechanism of pollutants (Zheng et al. 2017).

2 Measurements and methods

2.1 Lidar observation network

The vertical aerosol observation network of the NCP was composed of 13 aerosol lidar monitoring stations (Fig. 1), covering four main transport channels of Beijing pollutants, including the southwestern transport path of Baoding City (BD), Shijiazhuang City (SJZ), Xingtai City (XT), Handan City (HD), Xinxiang City (XX), and Yangquan City (YQ); the southern transport path of Dezhou City (DZ) and Jining City (JN); the southeastern transport path of Langfang City (LF), Cangzhou City (CZ), and Zibo City (ZB); the eastern transport path of Tianjin City (TJ); and a lidar in the urban area of Beijing (BJ).

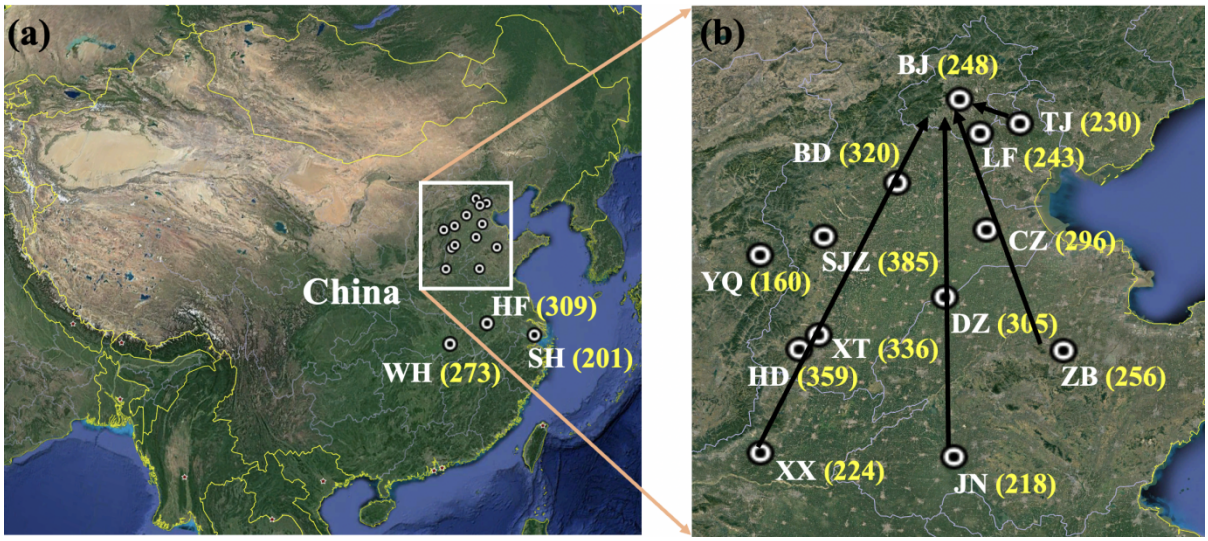

Figure 1. © Google maps of (a) China with the studied cities and (b) the North China Plain with all the lidar stations. The data in brackets are the maximum $PM_{2.5}$ concentrations ($\mu g \cdot m^{-3}$) at the surface during the observation period. The black arrows in (b, d) from left to right show that the main pollution pathways of Beijing come from the four directions of southwest, south, southeast, and east.

The lidar system was developed by the Anhui Institute of Optics and Fine Mechanics (AIOFM), Chinese Academy of Sciences (CAS), and was used for the long-term continuous observation of aerosol vertical distribution. The lidar system adopted the Nd: YAG laser, which emits a 532-nm wavelength, with 30-mJ single-pulse energy and 10–30-Hz pulse repetition frequency. The vertical resolution is 7.5 m, with the original time resolution of 3–10 min. The detection blind area is 0.1 km, and more specific technical details can be found in other literature (Xiang et al. 2019). The vertical distribution of the aerosol extinction coefficient was retrieved using the Fernald method (Fernald 1984), which is more suitable for vertical detection and more accurate than the Collis (Collis, Fernald, and Ligda 1964) and Klett (Klett 1981)

methods (Lu et al. 2015). Furthermore, combining the extinction coefficient with the $PM_{2.5}$ *in-situ* surface observations, the vertical distribution of the $PM_{2.5}$ mass concentration in the boundary layer was obtained using the empirical formula fitting method, which has proven to be reliable and highly accurate; the specific technical details can be found in other literature (Lv et al. 2017b; Tao et al. 2016; Lv et al. 2017a). In addition, an image recognition algorithm was used to evaluate the height of the atmospheric boundary layer (Xiang et al. 2019; Barrera et al. 2019).

2.2 WRF-Chem model configurations

The WRF-Chem chemical transport model (version 3.8.1) was used to investigate the particulate concentrations and meteorological parameters in the study area and was configured with nested domains consisting of 100 × 100 (36 km) and 103 × 103 (12 km) grids (Figs. S1). The domain had 41 vertical layers from the surface to 50 hPa. To better simulate the conditions within the boundary layer, the resolution of the boundary layer was increased, and 20 layers were set in the range of 0–2 km. The initial and boundary meteorological conditions were derived from the 6-h National Centers for Environmental Prediction Final Analysis data with 1° × 1° spatial resolution. The inventory of anthropogenic emissions for 2016 was obtained from the Multi-resolution Emission Inventory for China (MEIC) data with 0.25° × 0.25° resolution (Zhou et al. 2017). Terrestrial biogenic emissions were estimated using the Model of Emissions of Gases and Aerosols from Nature (MEGAN) model (Chatani et al. 2011). The gas-phase chemistry module CBM-Z and the Model for Simulating Aerosol Interactions and Chemistry (MOSAIC) aerosol module were used in this simulation. Detailed information concerning the model configuration is provided in Table S1. The model runs from November 20, 2017–December 9, 2017, and the results from November 25–December 9, 2017 were used for the analysis in Section 3.

2.3 GSI 3DVAR DA system

The GSI DA (Gridpoint Statistical Interpolation Data Assimilation) system provides 3DVAR analysis by minimizing the cost function as shown below (Gao, Saide, et al. 2017):

$$J(x) = (x - x_b)^T B^{-1}(x - x_b) + \big(y - H(x)\big)^T R^{-1}\big(y - H(x)\big) \quad (1)$$

In this equation, x is the analysis vector, x_b denotes the background vector, y is an observation vector, B represents the background error covariance matrix, R represents the observation error covariance matrix, and H is the observation operator used to transform model grid point values to observed variables, which was performed via interpolation in our research. The background error covariance matrix was calculated using the National Meteorological Center (NMC)

method (Parrish and Derber 1992; Saide et al. 2013), which simulated the difference of results at the same time (November 25, 2017) with two different starting times (November 20, 2017 and November 21, 2017, respectively). The 1-hour assimilated window data included 13 groups (see Fig. 1 for site distribution) of $PM_{2.5}$ vertical profiles retrieved from lidar, and the surface $PM_{2.5}$ data from hundreds of surface monitoring stations (see Fig. 5 for site distribution) from the China Environmental Monitoring Center. The observation errors of $PM_{2.5}$ ground and its vertical distribution (through the ground $PM_{2.5}$ fitting method in Section 2.1) originated from measurement errors and representative errors. The measurement error was computed using $\varepsilon_0 = 1.5 + 0.0075 * obs$ (Pagowski et al. 2014), where *obs* indicates observed values. The representative error was computed using $\varepsilon_r = \gamma\varepsilon_0\sqrt{\Delta x/L}$ (Elbern et al. 2007), where γ is the adjustable scale factor (we used the value of 0.5 recommended by the GSI system), Δx is the model grid resolution (we selected 12 km of domain 2), and L is the influencing radius (we used 60 km).

3 Results and discussion

3.1 Evaluation of assimilation performance using vertical $PM_{2.5}$ data

In order to evaluate the improvement of model simulation performance from data assimilation using lidar vertical profile data and surface station data, considering the sharp decline of $PM_{2.5}$ value at 1 km height (Fig. 6), only the non-assimilation and assimilation results at the surface, 0.2 km, 0.5 km, and 1 km were compared, as shown in Fig. 2. These data were selected from five of the most polluted stations, including the cities of TJ, LF, BD, SJZ, and XT. It should be noted that these observation data were not assimilated, which means that the following comparisons are independent (Bocquet et al. 2015). Obviously, the data assimilation used can greatly improve the simulation accuracy. Compared with the observation data at different heights (ground, 0.2, 0.5 and 1 km), the simulation results of $PM_{2.5}$ levels under the condition of non-assimilation were higher (Figs. 2 a–d), the root-mean-square error (RMSE) was 52.14 ± 20.27 $\mu g \cdot m^{-3}$, and the correlation coefficient was only 0.56 ± 0.15. Correspondingly, the results of $PM_{2.5}$ simulated with assimilation were closer to the observed values (Figs. 2 e–h), the RMSE was 33.07 ± 14.69 $\mu g \cdot m^{-3}$, which represents a reduction of about 40% in simulation error after assimilation. The correlation coefficient was 0.81 ± 0.10, demonstrating that the simulation accuracy was improved by about 50% after assimilation.

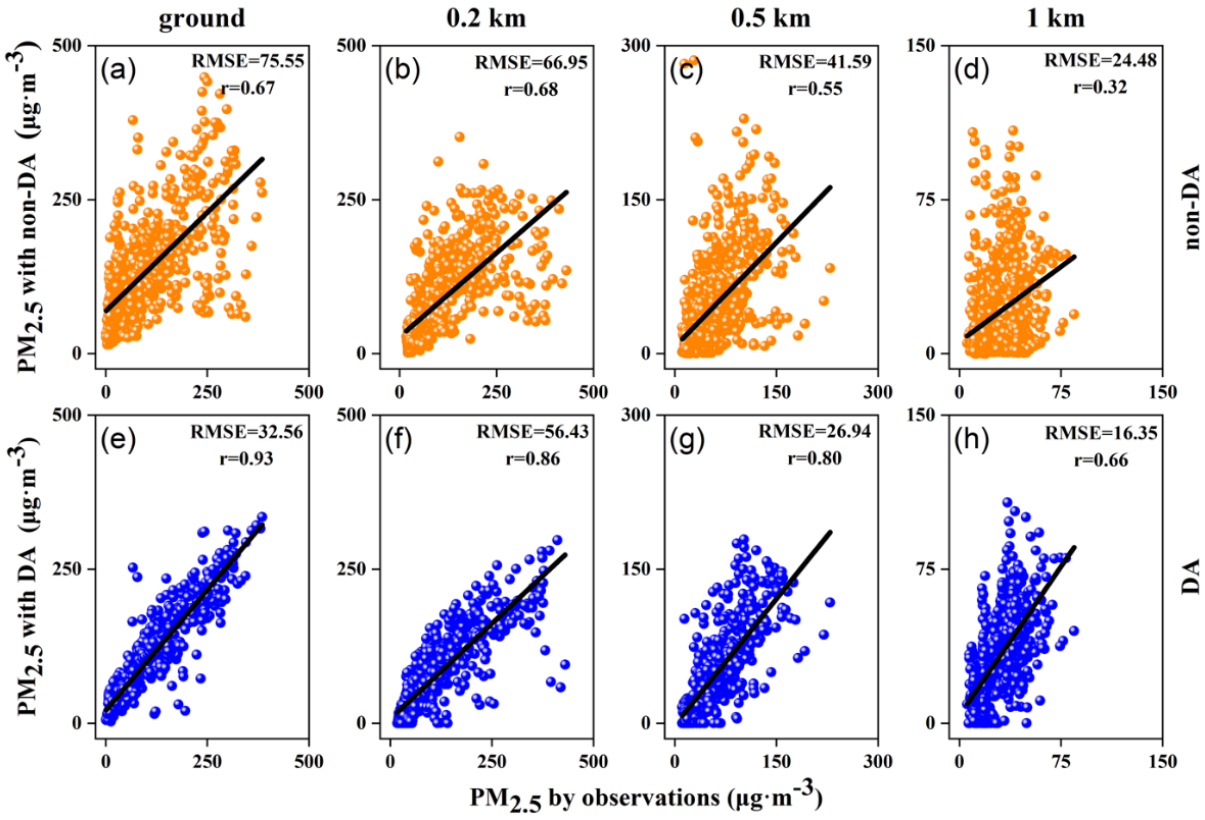

Figure 2. $PM_{2.5}$ mass concentration comparison results from lidar at different heights (b–d, f–h) and surface observations (a, e) with non-assimilation simulations (a–d) and assimilation simulations (e–h).

In addition, compared with the simulation with assimilation (Fig. 5 in Section 3.3), the results without assimilation were significantly higher than the observed values (Fig. S2), especially during the pollution period (Figs. S2d, S2e), which may be due to the simulation error caused by the model (Zhang et al. 2016). Meanwhile, the comparison of the three-dimensional results (Fig. 7 in Section 3.5 and Fig S3) further reveals that the simulation results of upper air $PM_{2.5}$ may also overestimate the actual values, which demonstrates the importance of data assimilation in capturing the three-dimensional structure of pollution.

3.2 The four phases from aerosol pollution development to dissipation

Joint observations and analyses have been widely performed in an effort to reveal the heavy aerosol pollution (HAP) in the NCP region (Li et al. 2016; Zhang et al. 2018). The key processes of a HAP event, from aerosol pollution development to dissipation, usually include an early phase (EP), a transport phase (TP), an accumulation phase (AP), and a removal phase (RP) (Yuan et al. 2019; Zhong et al. 2017), classifications that are based on the increase and decrease of $PM_{2.5}$ mass concentration in Beijing (BJ) caused by changes in meteorological conditions. Here, the curves in Fig. 3 shows the temporal evolution of $PM_{2.5}$ mass concentration monitored at the surface in different cities on the NCP from November 25–December 9, 2017,

while the superimposed colors represent the time-varying profiles of the simulated wind fields in BJ, Baoding (BD), Dezhou (DZ), and Langfang (LF), respectively. Overall, $PM_{2.5}$ with high concentrations was usually associated with pronounced southerly winds (S in Fig. 3) or southwesterly winds (SW in Fig. 3), while the $PM_{2.5}$ concentrations decreased significantly under the prevailing northerly winds (including the wind directions of N, NW, and NE in Fig. 3).

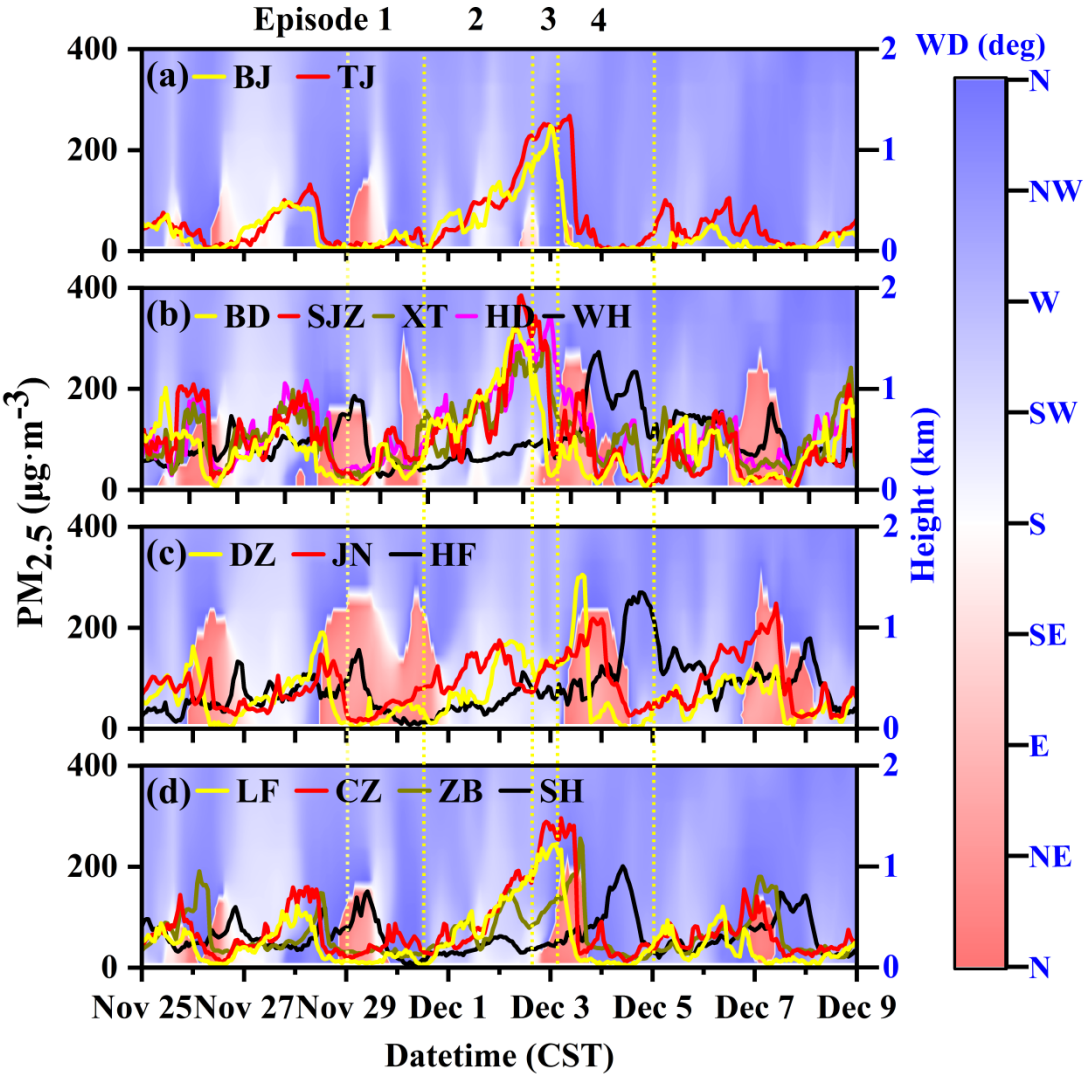

Figure 3. Surface $PM_{2.5}$ observations from different cities: (a) Beijing (including Tianjin) and its (b) southwest cities, (c) southeast cities, and (d) east cities for the period November 25–December 9, 2017. Superimposed colors represent the time-varying profiles of the simulated wind fields in Beijing, Baoding, Dezhou, and Langfang, respectively.

Furthermore, in order to characterize the evolution of $PM_{2.5}$ during different pollution phases, the period from November 29–December 5 was selected as a typical extreme HAP event covering the four pollution phases. This extreme pollution event lasted more than 4 days and featured a regional transport process. During the EP (November 29–noon November 30;

episode 1 in Fig. 3), the air quality in BJ and its surrounding areas such as Tianjin (TJ) was relatively good, with an average $PM_{2.5}$ value of ~15 $\mu g \cdot m^{-3}$, while slight pollution occurred to the southwest of BJ, including BD, Shijiazhuang (SJZ), Xingtai (XT), and Handan (HD), with an average value of ~50 $\mu g \cdot m^{-3}$.

During the TP (approximately the morning of December 2; episode 2 in Fig. 3), the variation of $PM_{2.5}$ concentration was more sensitive and responded rapidly to the wind shift from northerly to southerly, causing the $PM_{2.5}$ concentration in Beijing to increase quickly from ~30 $\mu g \cdot m^{-3}$ to ~150 $\mu g \cdot m^{-3}$, while southwest of Beijing (e.g., BD, SJZ, XT, and HD) the $PM_{2.5}$ concentration increased rapidly to ~200 $\mu g \cdot m^{-3}$. Research has revealed that the pollutant transport south of Beijing, especially in the southwest areas (the Taihang Mountains), is the most important contribution source of Beijing pollutants (Zhao et al. 2020). During the AP (approximately December 3; episode 3 in Fig. 3), diffusion of the pollutants was difficult due to the occurrence of a surface temperature inversion in Beijing (Fig. 4) (Wang et al. 2019), which caused the maximum concentration of $PM_{2.5}$ in Beijing to reach ~250 $\mu g \cdot m^{-3}$. Meanwhile, the $PM_{2.5}$ concentrations in TJ, LF, BD, and SJZ reached maximum values of ~270, 250, 320, and 390 $\mu g \cdot m^{-3}$, respectively. Conversely, the pollution levels in Shanghai (SH), Hefei (HF), and Wuhan (WH) in the southernmost section of the NCP were relatively low, with average values < ~60 $\mu g \cdot m^{-3}$.

During the RP (approximately December 5; episode 4 in Fig. 3), the wind direction shifted from southwest to north, transporting the relatively clean air in the north to the south, and thereby causing the pollutant concentrations in Beijing to decrease rapidly. In just 9 hours, the air quality improved from heavy pollution to excellent, and the $PM_{2.5}$ concentrations in the NCP also decreased significantly. Finally, by noon on December 4, the pollutant concentrations in the NCP had reached a low level, with an average value of ~40 $\mu g \cdot m^{-3}$. In contrast, due to the continuous southward advection of pollutants, serious pollution occurred in SH, HF, and WH, where the $PM_{2.5}$ concentrations reached maximum values of ~210, 310, and 280 $\mu g \cdot m^{-3}$, respectively. These findings are also consistent with the results of previous studies on the regional transport of regional pollutants to the Yangtze River Delta (Hua et al. 2015), which showed them to be due to the continuous southward flow of northwest and northeast winds.

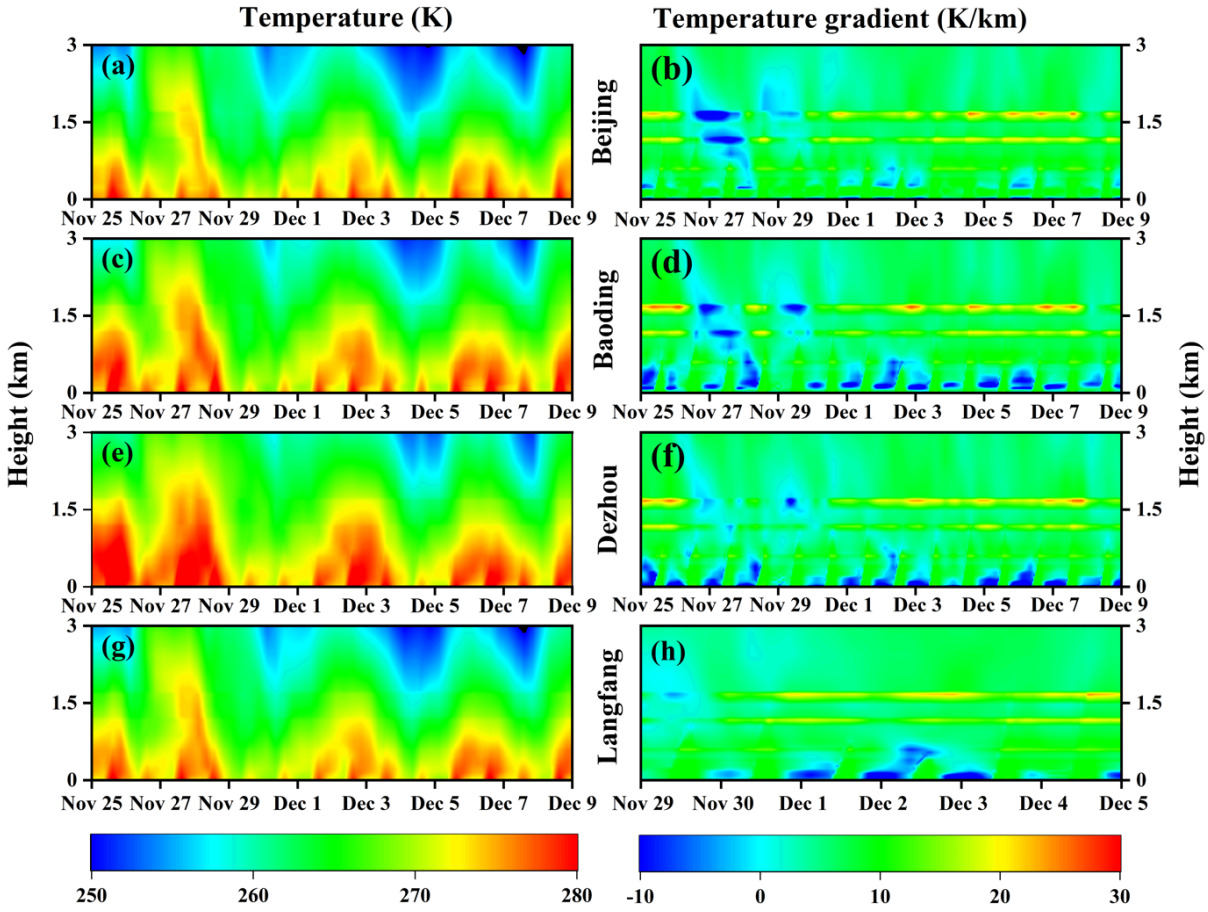

Figure 4. Time series of vertical temperatures (a, c, e, g) and temperature gradients (b, d, f, h) from Beijing (a, b), Baoding (c, d), Dezhou (e, f), and Langfang (g, h) simulated by the WRF-Chem model.

3.3 Spatial distribution of $PM_{2.5}$ concentration in the surface layer

Additionally, in order to analyze the pollution characteristics of the NCP, the spatial distribution results of $PM_{2.5}$ after data assimilation were plotted in Fig. 5 for all phases. The high concentrations of $PM_{2.5}$ in BJ were recorded during the TP, AP, and beginning of the RP, while the $PM_{2.5}$ concentrations at other times were lower. Moreover, during the EP, only the eastern cities of Shanxi (SX) Province experienced moderate pollution levels (Fig. 5a). During the TP, the pollutants in the south-central NCP were transported to the north of the NCP (Figs. 5b and c) as a result of the southwesterly wind field, and under the superposition of the local pollutant emissions from each city (Li, Du, et al. 2017), the cities on the windward side of the Taihang Mountains (e.g., HD, SJZ, and BD) quickly developed varying levels of heavy pollution. In addition, during the AP, due to the large-scale inversion (Figs. 4b, d, f, h) caused by the rapid temperature rise (Figs. 4a, c, e, g) of the NCP region at upper levels, the atmospheric stratification was stable, causing the pollutant loading on the NCP (including BJ, BD, SJZ, HD, LF, CZ, and elsewhere) to increase (Fig. 5d), nearly reaching their pollution maxima (Fig. 3). Meanwhile, during the RP, affected by the cold air at upper levels (Figs. 4a,

c, e, g) from the northwest and the shift in wind direction over the NCP from southwest to north, the pollution severity gradually eased from north to south (Fig. 5e), with the air quality in the northern part of the region improving significantly (Fig. 5f).

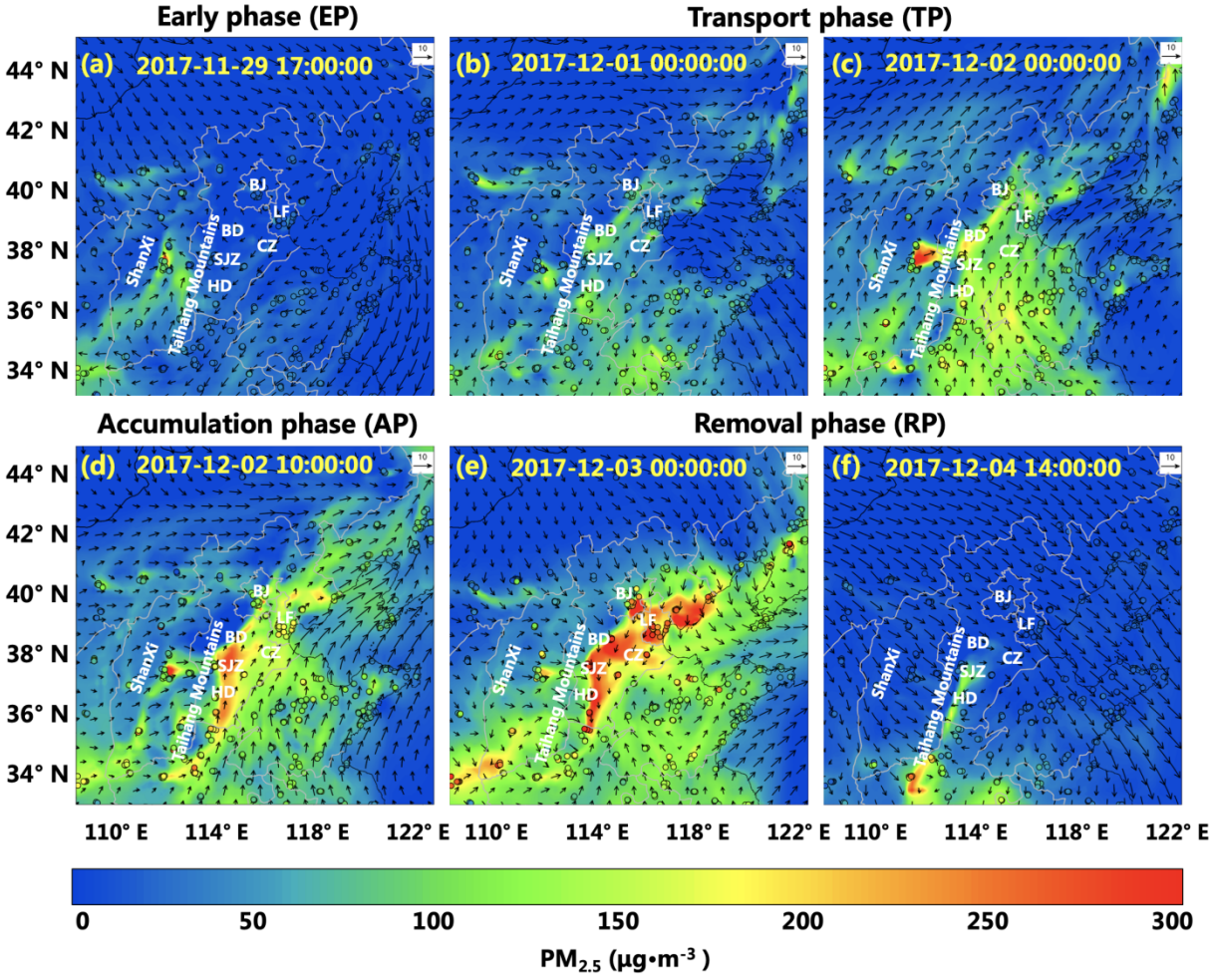

Figure 5. Spatial distribution of $PM_{2.5}$ in the surface layer during different phases after assimilation. The black arrows indicate the wind direction. The circles represent the *in-situ* surface observations.

3.4 Vertical distribution of aerosols observed by the lidar network

In order to quantify the characteristic vertical distribution of aerosols, the observed aerosol extinction coefficients from the 13 lidar stations in the NCP were plotted, as shown in Fig. 6. These results revealed that on November 29, the aerosol concentration at the surface was relatively low, although pollutant transport at heights of 1–2 km (see Figs. 8a, e) occurred at six stations (BD, SJZ, YQ, XT, HD, and XX) on the windward side of the Taihang Mountains. Figure S4 demonstrates that these pollutants in the upper air come from the local emissions on the ground, which is due to the updraft lifting to 1-2 km above the ground on the night of November 28. The upper air transport of pollutants continued until December 1, at which it merged with the surface flow. Contrary to this, the pollutant transport from north to south occurred at a height of 1 km during the RP (e.g., Figs. 6b, d–g). In addition, the atmospheric

boundary layer height (ABLH) reached its highest value of the observation period from November 29 to 30, averaging more than 1.5 km. The ABLH began to decrease on December 1, averaging approximately 1 km on that day. The lowest value of the ABLH occurred on December 2–3, when its average dropped to less than 0.5 km, making it difficult for pollutants to diffuse and causing heavy pollution in the NCP (Li, Guo, et al. 2017). Fortunately, on December 4, the atmospheric boundary layer gradually lifted, which was conducive to the diffusion of pollutants.

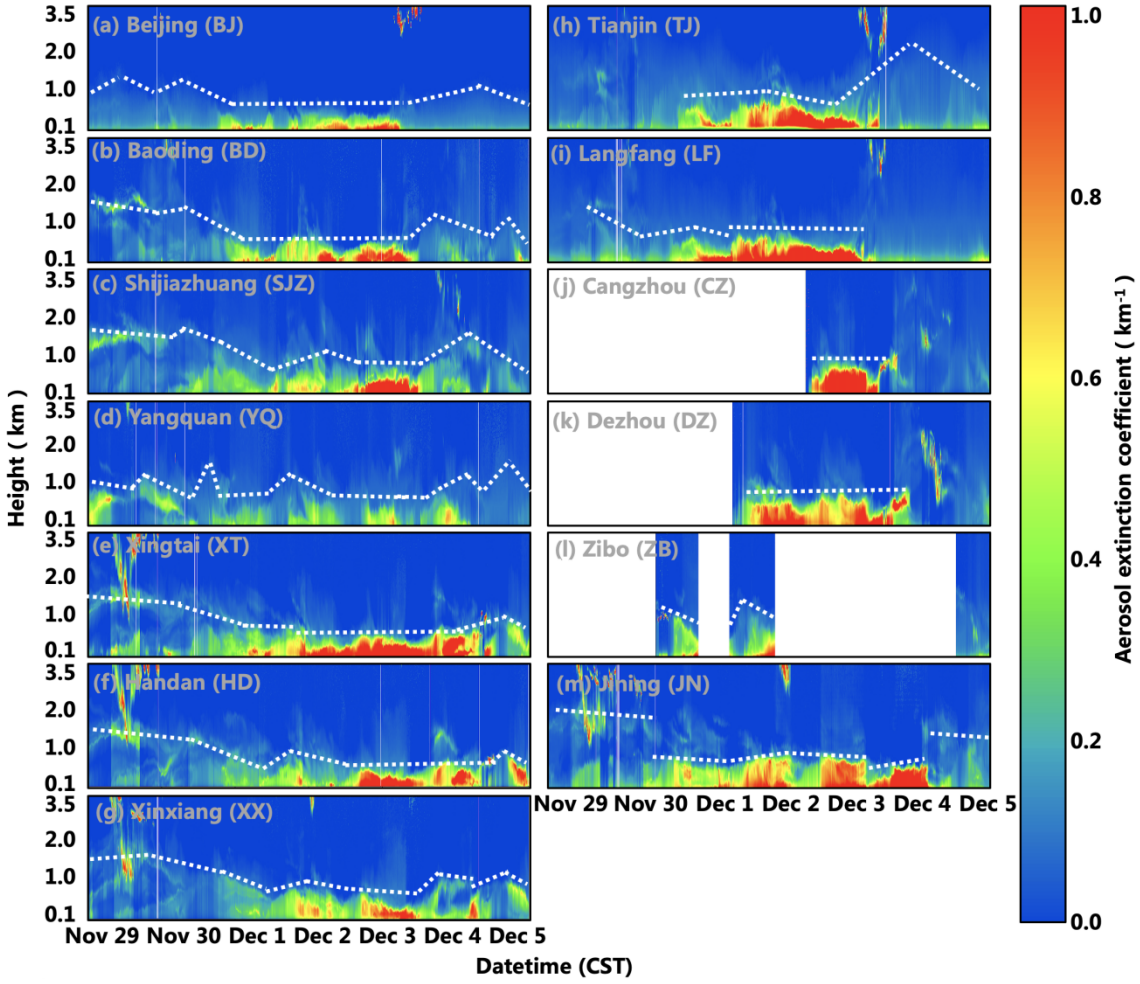

Figure 6. Time series of vertical distributions of the aerosol extinction coefficient observed on the North China Plain from November 29–December 5, 2017. The white dashed lines represent the approximate atmospheric boundary layer height. Missing datasets are plotted in white.

3.5 Dynamic 3-D evolution of the $PM_{2.5}$ concentrations

Figure 7 presents the 3-D distribution of $PM_{2.5}$ after assimilation, which clearly shows the generation, dissipation, transport, and diffusion characteristics of pollutants in the atmosphere. The tops of the boxes in the figure depict the wind speeds 10 m above the surface. During the EP, the high-concentration pollutants only occurred in the upper air within ~1 km of the surface in SX Province (e.g., YQ). During the TP, the high-concentration pollutants were

mainly found on the windward side of the Taihang Mountains (southwest pathway), and the loading height of $PM_{2.5}$ was < 1 km, which is illustrated in Fig. 8. During the AP, the average concentration of pollutants > 200 $\mu g \cdot m^{-3}$ mainly occurred near the surface. Meanwhile, the pollutants with low concentrations at upper levels could be transported to the Bohai Sea. During the RP, high-concentration pollutants > 100 $\mu g \cdot m^{-3}$ simultaneously occurred over the Bohai Sea and the Yellow Sea.

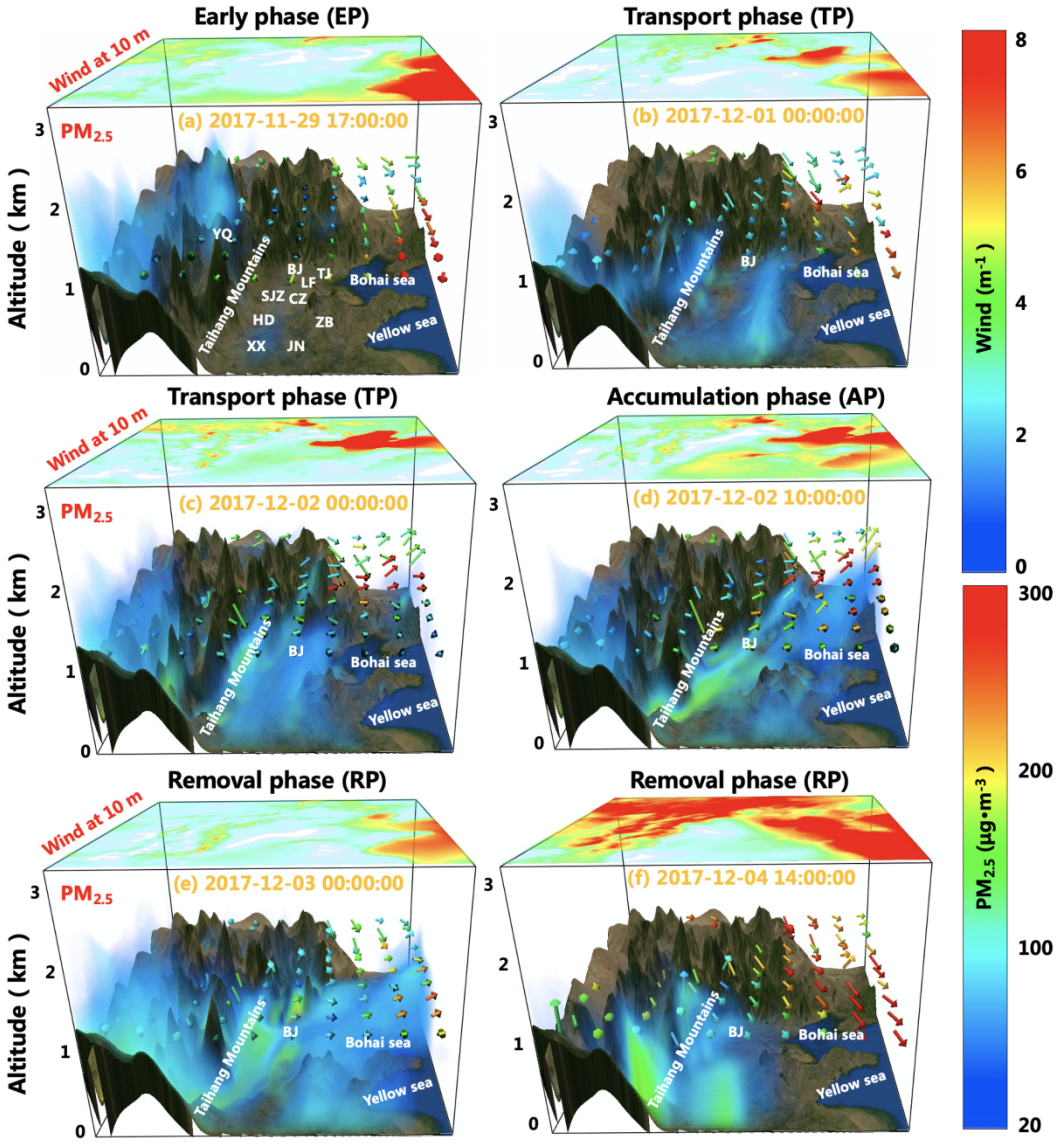

Figure 7. Three-dimensional distribution of $PM_{2.5}$ during different phases after assimilation. Colors within the boxes depict the $PM_{2.5}$ concentrations. The color-coded arrows represent the wind direction and speed at 1 km. On the tops of the boxes, the spatial distributions of wind speed at 10 m are plotted.

3.6 Quantification of regional transport of $PM_{2.5}$

To evaluate the variation of pollutants along different transport pathways at different stages, we plotted the vertical profile of the $PM_{2.5}$ cross-section along the main pollution pathways of Beijing coming from the four directions of southwest, south, southeast, and east

(see Figs. 1b, d). As shown in Fig.8, at XX and XT (located at the start of the southwest transport pathway, Fig. 8a), the $PM_{2.5}$ concentration is more than 200 $\mu g \cdot m^{-3}$ at a height of 1 km (Fig. 8a), and the surface $PM_{2.5}$ concentration at JN (located in the south pathway) also exceeds 200 $\mu g \cdot m^{-3}$ (Fig. 8b). These high concentrations of pollutants were transported to SJZ, BD, LF, BJ, and other cities via southwest winds (Figs. 8e, f, g). At the same time, vertical downdrafts reduced the height of loading of aerosol layer to ~0.6 km (Fig. 8e). Different from the southern (including southwest, south, and southeast) transport pathways, the pollutants in TJ were mainly from BJ outflow in all stages of the eastern transport pathways (Figs. 8d, h, l, p). In addition, wind direction inconsistencies at the origin (XX, JN, and ZB) and target location (Beijing) of the transport pathways occurred at the beginning of the removal phase (Figs. 8i–k), which may have been due to the southward delay of the northerly air flow.

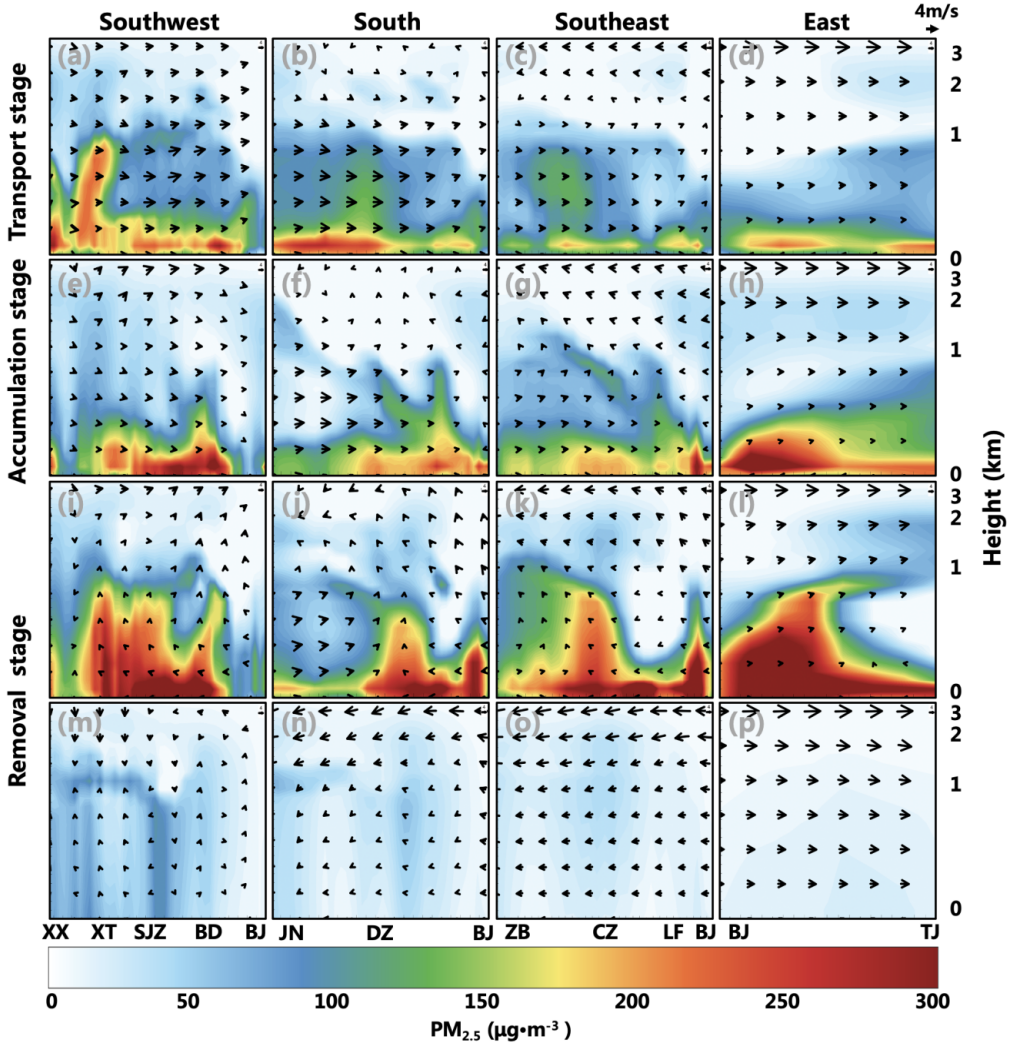

Figure 8. Vertical profiles of $PM_{2.5}$ cross-sections with wind vectors along the transport pathways, including southwest (first column), south (second column), southeast (third column), and east (fourth column). The first row (00:00 December 2, 2017) represents the transport stage, the second row (10:00 December 2, 2017) represents the accumulation stage, the third row (00:00, December 3, 2017) and the fourth row (14:00, December 4, 2017) represent the removal stage.

To investigate the vertical variation of $PM_{2.5}$ inflow or outflow at different heights and determine the height at which the main transport occurred (Zhang, Cheng, et al. 2019), we plotted the vertical distribution of $PM_{2.5}$ transport flux in different directions (Fig. 9). Here the $PM_{2.5}$ transport flux is defined as the product of $PM_{2.5}$ mass concentration ($\mu g\ m^{-3}$), wind speed ($m\ s^{-1}$), and wind direction projection in the current pathway (Xiang et al. 2020). The southwest, southeast, and east pathways in Fig. 9 were represented by BD, LF, and TJ, respectively, which are the three lidar stations closest to BJ (Fig. 1). TF > 0 indicates that the pollutants were imported to Beijing, while TF < 0 indicates that the pollutants were exported from Beijing. The results revealed that below the height of 3 km, the order of the maximum values of imported pollutants to Beijing direction was southwest pathway (1122.8 $\mu g\ m^{-2}\ s^{-1}$) > southeast pathway (423.6 $\mu g\ m^{-2}\ s^{-1}$) > east pathway (278.3 $\mu g\ m^{-2}\ s^{-1}$), while the exported pollutants from Beijing direction was southwest pathway (-1571.4 $\mu g\ m^{-2}\ s^{-1}$) > east pathway (-877.7 $\mu g\ m^{-2}\ s^{-1}$)> southeast pathway (-772.4 $\mu g\ m^{-2}\ s^{-1}$). Compared with the $PM_{2.5}$ transport flux on the ground surface, the relatively high value (~ 200 $\mu g\ m^{-2}\ s^{-1}$) in the southwest pathway (Fig. 9a) occurred on November 29 and early morning on December 4, while the relatively extreme value (~ -400 $\mu g\ m^{-2}\ s^{-1}$) on the east pathway (Fig. 9c) was recorded at the night of December 2.

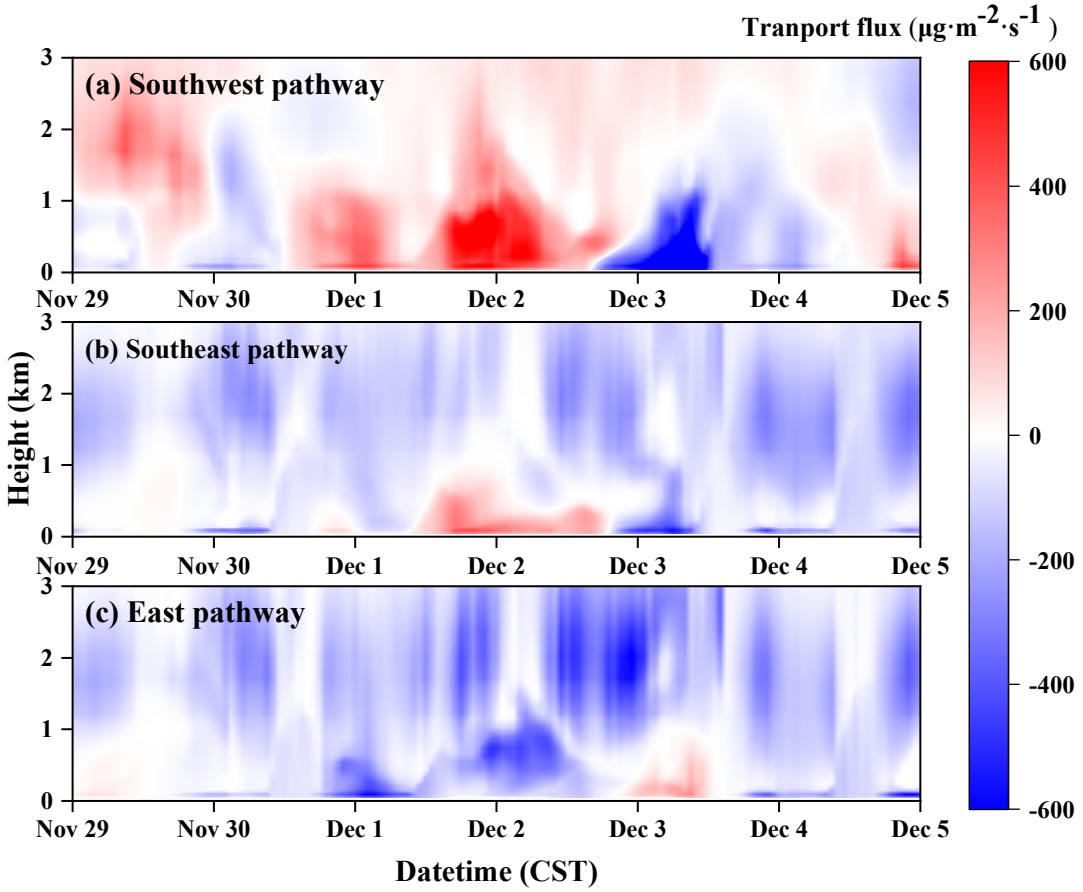

Figure 9. Time series of $PM_{2.5}$ transport flux from different transport pathways. The corresponding directions of the southwest, southeast, and east pathways are shown in Fig. 1.

To further obtain insights into the total transport characteristics in the target area (BJ) and its surrounding area (BD, LF, and TJ) during different evolutionary stages, the time series of the $PM_{2.5}$ transport flux intensity (TFI) was shown in Fig. 10. The TFI was calculated by integrating the $PM_{2.5}$ transport flux from the ground to a certain height, and the height was selected as 1.5 km, which is consistent with the main transport height of pollutants (Fig. 8) and the height of boundary layer (Fig. 7). The TFI of $PM_{2.5}$ further reveals that pollutants imported into the Beijing area with a maximum $PM_{2.5}$ TFI of ~4.6×10^5 $\mu g \cdot m^{-1} \cdot s^{-1}$ were transported mainly via the southwest pathway during the TP, while the extreme TFI of pollutants exported from Beijing via the east pathway was approximately -1.4×10^5 $\mu g \cdot m^{-1} \cdot s^{-1}$. In addition, during the RP, the pollutants from Beijing were exported to the southwest and southeast, with extreme values of approximately -1.03×10^6 and -4.3×10^5 $\mu g \cdot m^{-1} \cdot s^{-1}$, respectively. In contrast, the absolute value of TFI on the southwest pathway was < ~1.0×10^4 $\mu g \cdot m^{-1} \cdot s^{-1}$ during the EP (Fig. 10), which indicates that there was no significant inflow or outflow of pollutants. However, this reason was mainly due to the offsetting of the inflow of pollutants in the upper-air and the outflow of pollutants near the ground (Fig. 9a). This special phenomenon also demonstrates that the study of vertical distribution of pollutants has great significance, which can better explain the transport characteristics (Zhang, Cheng, et al. 2019).

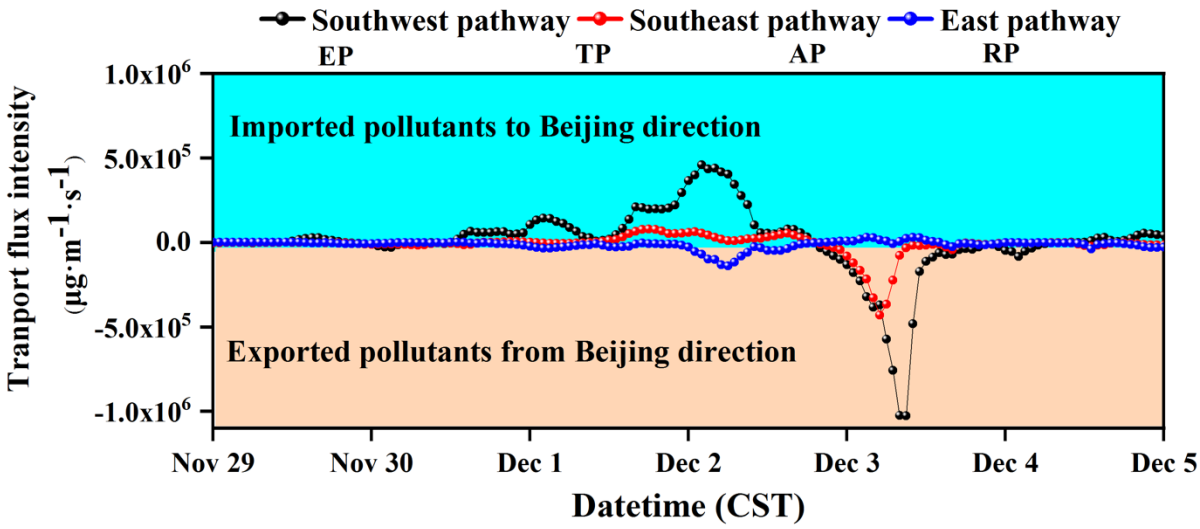

Figure 10. Time series of $PM_{2.5}$ transport flux intensity from different transport pathways. The corresponding directions of the southwest, southeast, and east pathways are shown in Fig. 1.

4 Conclusions

Accurate quantification of the distribution of particulate matter in the atmosphere is a key requirement for predicting air quality and estimating atmospheric environmental capacity from atmospheric observations. We utilized a vertical observation network composed of 13

aerosol lidars, combined with data assimilation technology, to improve the simulation accuracy of $PM_{2.5}$, and further analyzed the multi-dimensional evolutionary characteristics of pollutants in the surface layer, vertical layer, and 3-D space, thereby providing effective data support for clarifying the spatial transport characteristics of heavy pollution.

We found that the average height of the atmospheric boundary layer was < 0.5 km during the HAP period. We further demonstrated that the transport of pollutants in the NCP region was mainly via three pathways: southwest, southeast, and east. During the TP, the $PM_{2.5}$ advected into Beijing with a maximum transport flux intensity (TFI) of ~4.6×10^5 $\mu g\cdot m^{-1}\cdot s^{-1}$ was mainly via the southwest pathway, while the polluted air mass in the RP dissipated from Beijing via the southwest and southeast pathways, with extreme $PM_{2.5}$ TFI values of approximately -1.03×10^6 and -4.3×10^5 $\mu g\cdot m^{-1}\cdot s^{-1}$, respectively. In addition, the transport of regional pollutants to the Yangtze River Delta was due to the continuous southward flow of northwest and northeast winds. Our results directly revealed that pollutants in the North China Plain can be transported to the Yellow Sea and the Bohai Sea, providing a dataset for a further in-depth study of the mechanism of air pollution in the coastal areas of eastern China. This study also captured the regional transport of air pollutants stretching over 1000 km, proving the necessity and importance of the joint prevention and control of regional air pollution.

Data availability

The FNL data are available from the following website (https://rda.ucar.edu/datasets/ds083.2/). The data in this study are analyzed using the NCAR Command Language (http://www.ncl.ucar.edu/). The authors are gratefully acknowledging the China National Environmental Monitoring Center for providing monitoring data for the $PM_{2.5}$ (http://106.37.208.233:20035). The lidar data in this study are available upon request from the corresponding author (yxiang@ahu.edu.cn).

Author contributions

YX and TZ designed this study. YX wrote the manuscript; YC and CM edited it. LL and TZ helped to analyze the data. YC, CM, WL, and JL provided constructive comments on this study. All authors contributed to the discussion and final version of the manuscript.

Competing interests

The authors declare that they have no conflict of interest.

Acknowledgements

This work was supported by the National Natural Science Foundation of China (42005106, 41941011), and the National Key Project of MOST (2017YFC0213002, 2018YFC0213101, 2018YFC0213106, 2018YFC0213201), and the Major science and technology projects of Anhui Province (No.18030801111), and the Natural Science Foundation of Anhui Province, China (1908085QD160, 1908085QD170), and the Doctoral Scientific Research Foundation of Anhui University (Y040418190). The authors are grateful to the China National Environmental Monitoring Center for providing the $PM_{2.5}$ monitoring data. The authors acknowledge the High-performance Computing Platform of Anhui University for providing computing resources. The authors also gratefully acknowledge © Google Earth for providing the map used in this research. Yafang Cheng and Chaoqun Ma thank the Minerva program of Max Planck Society.

References

Barrera, Y. D., T. Nehrkorn, J. Hegarty, M. Sargent, J. Benmergui, E. Gottlieb, S. C. Wofsy, P. DeCola, L. Hutyra, and T. Jones. 2019. 'Using Lidar Technology To Assess Urban Air Pollution and Improve Estimates of Greenhouse Gas Emissions in Boston', *Environmental Science & Technology*, 53: 8957-66.

Bocquet, M., H. Elbern, H. Eskes, M. Hirtl, R. Zabkar, G. R. Carmichael, J. Flemming, A. Inness, M. Pagowski, J. L. P. Camano, P. E. Saide, R. San Jose, M. Sofiev, J. Vira, A. Baklanov, C. Carnevale, G. Grell, and C. Seigneur. 2015. 'Data assimilation in atmospheric chemistry models: current status and future prospects for coupled chemistry meteorology models', *Atmospheric Chemistry And Physics*, 15: 5325-58.

Cao, F., Y. L. Zhang, L. J. Ren, J. W. Liu, J. Li, G. Zhang, D. Liu, Y. L. Sun, Z. F. Wang, Z. B. Shi, and P. Q. Fu. 2017. 'New insights into the sources and formation of carbonaceous aerosols in China: potential applications of dual-carbon isotopes', *National Science Review*, 4: 804-+.

Chatani, S., T. Morikawa, S. Nakatsuka, S. Matsunaga, and H. Minoura. 2011. 'Development of a framework for a high-resolution, three-dimensional regional air quality simulation and its application to predicting future air quality over Japan', *Atmospheric Environment*, 45: 1383-93.

Che, Huizheng, Ke Gui, Xiangao Xia, Yaqiang Wang, Brent N. Holben, Philippe Goloub, Emilio Cuevas-Agulló, Hong Wang, Yu Zheng, Hujia Zhao, and Xiaoye Zhang. 2019. 'Large contribution of meteorological factors to inter-decadal changes in regional aerosol optical depth', *Atmospheric Chemistry And Physics*, 19: 10497-523.

Che, Huizheng, Xiangao Xia, Hujia Zhao, Oleg Dubovik, Brent N. Holben, Philippe Goloub, Emilio Cuevas-Agulló, Victor Estelles, Yaqiang Wang, Jun Zhu, Bing Qi, Wei Gong, Honglong Yang, Renjian Zhang, Leiku Yang, Jing Chen, Hong Wang, Yu Zheng, Ke Gui, Xiaochun Zhang, and Xiaoye Zhang. 2019. 'Spatial distribution of aerosol microphysical and optical properties and direct radiative effect from the China Aerosol Remote Sensing Network', *Atmospheric Chemistry And Physics*, 19: 11843-64.

Chen, D., Z. Q. Liu, J. M. Ban, and M. Chen. 2019. 'The 2015 and 2016 wintertime air pollution in China: SO2 emission changes derived from a WRF-Chem/EnKF coupled data assimilation system', *Atmospheric Chemistry And Physics*, 19: 8619-50.

Chen, D. S., X. X. Liu, J. L. Lang, Y. Zhou, L. Wei, X. T. Wang, and X. R. Guo. 2017. 'Estimating the contribution of regional transport to PM2.5 air pollution in a rural area on the North China Plain', *Science of the Total Environment*, 583: 280-91.

Chen, Z., R. Schofield, P. Rayner, T. Zhang, C. Liu, C. Vincent, S. Fiddes, R. G. Ryan, J. Alroe, Z. D. Ristovski, R. S. Humphries, M. D. Keywood, J. Ward, C. Paton-Walsh, T. Naylor, and X. Shu. 2019. 'Characterization of aerosols over the Great Barrier Reef: The influence of transported continental sources', *Science of the Total Environment*, 690: 426-37.

Cheng, X., Y. Liu, X. Xu, W. You, Z. Zang, L. Gao, Y. Chen, D. Su, and P. Yan. 2019. 'Lidar data assimilation method based on CRTM and WRF-Chem models and its application in PM2.5 forecasts in Beijing', *Science Of the Total Environment*, 682: 541-52.

Cheng, Y. F., G. J. Zheng, C. Wei, Q. Mu, B. Zheng, Z. B. Wang, M. Gao, Q. Zhang, K. B. He, G. Carmichael, U. Poschl, and H. Su. 2016. 'Reactive nitrogen chemistry in aerosol water as a source of sulfate during haze events in China', *Science Advances*, 2,e1601530.

Collis, Ronald T. H, Frederick G Fernald, and Myron G. H Ligda. 1964. 'Laser Radar Echoes from a Stratified Clear Atmosphere', *Nature*.

Dong, Z., S. Wang, J. Xing, X. Chang, D. Ding, and H. Zheng. 2020. 'Regional transport in Beijing-Tianjin-Hebei region and its changes during 2014-2017: The impacts of meteorology and emission reduction', *Science of the Total Environment*, 737: 139792.

Elbern, H., A. Strunk, H. Schmidt, and O. Talagrand. 2007. 'Emission rate and chemical state estimation by 4-dimensional variational inversion', *Atmospheric Chemistry And Physics*, 7: 3749-69.

Fan, W. Z., K. Qin, J. Xu, L. M. Yuan, D. Li, Z. Jin, and K. F. Zhang. 2019. 'Aerosol vertical distribution and sources estimation at a site of the Yangtze River Delta region of China', *Atmospheric Research*, 217: 128-36.

Fernald, F. G. 1984. 'Analysis of Atmospheric Lidar Observations - Some Comments', *Applied Optics*, 23: 652-53.

Gao, J. H., A. Woodward, S. Vardoulakis, S. Kovats, P. Wilkinson, L. P. Li, L. Xu, J. Li, J. Yang, J. Li, L. Cao, X. B. Liu, H. X. Wu, and Q. Y. Liu. 2017. 'Haze, public health and mitigation measures in China: A review of the current evidence for further policy response', *Science of the Total Environment*, 578: 148-57.

Gao, M., P. E. Saide, J. Y. Xin, Y. S. Wang, Z. R. Liu, Y. X. Wang, Z. F. Wang, M. Pagowski, S. K. Guttikunda, and G. R. Carmichael. 2017. 'Estimates of Health Impacts and Radiative Forcing in Winter Haze in Eastern China through Constraints of Surface PM2.5 Predictions', *Environmental Science & Technology*, 51: 2178-85.

Heese, B., H. Baars, S. Bohlmann, D. Althausen, and R. R. Deng. 2017. 'Continuous vertical aerosol profiling with a multi-wavelength Raman polarization lidar over the Pearl River Delta, China', *Atmospheric Chemistry And Physics*, 17: 6679-91.

Hong, Q. Q., C. Liu, K. L. Chan, Q. H. Hu, Z. Q. Xie, H. R. Liu, F. Q. Si, and J. G. Liu. 2018. 'Ship-based MAX-DOAS measurements of tropospheric NO2, SO2, and HCHO distribution along the Yangtze River', *Atmospheric Chemistry And Physics*, 18: 5931-51.

Hu, M., S. Guo, J. F. Peng, and Z. J. Wu. 2015. 'Insight into characteristics and sources of PM2.5 in the Beijing-Tianjin-Hebei region, China', *National Science Review*, 2: 257-58.

Hua, Y., Z. Cheng, S. X. Wang, J. K. Jiang, D. R. Chen, S. Y. Cai, X. Fu, Q. Y. Fu, C. H. Chen, B. Y. Xu, and J. Q. Yu. 2015. 'Characteristics and source apportionment of PM2.5

during a fall heavy haze episode in the Yangtze River Delta of China', *Atmospheric Environment*, 123: 380-91.

Huang, M., J. H. Crawford, G. S. Diskin, J. A. Santanello, S. V. Kumar, S. E. Pusede, M. Parrington, and G. R. Carmichael. 2018. 'Modeling Regional Pollution Transport Events During KORUS-AQ: Progress and Challenges in Improving Representation of Land-Atmosphere Feedbacks', *Journal Of Geophysical Research-Atmospheres*, 123: 10732-56.

Huang, X., L. X. Zhou, A. J. Ding, X. M. Qi, W. Nie, M. H. Wang, X. G. Chi, T. Petaja, V. M. Kerminen, P. Roldin, A. Rusanen, M. Kulmala, and M. Boy. 2016. 'Comprehensive modelling study on observed new particle formation at the SORPES station in Nanjing, China', *Atmospheric Chemistry And Physics*, 16: 2477-92.

Huang, Xin, Zilin Wang, and Aijun Ding. 2018. 'Impact of Aerosol-PBL Interaction on Haze Pollution: Multiyear Observational Evidences in North China', *Geophysical Research Letters*, 45: 8596-603.

Jiang, Z. Q., Z. Q. Liu, T. J. Wang, C. S. Schwartz, H. C. Lin, and F. Jiang. 2013. 'Probing into the impact of 3DVAR assimilation of surface PM10 observations over China using process analysis', *Journal of Geophysical Research-Atmospheres*, 118: 6738-49.

Klett, J. D. 1981. 'Stable Analytical Inversion Solution for Processing Lidar Returns', *Applied Optics*, 20: 211-20.

Kumar, M., M. P. Raju, R. K. Singh, A. K. Singh, R. S. Singh, and T. Banerjee. 2017. 'Wintertime characteristics of aerosols over middle Indo-Gangetic Plain: Vertical profile, transport and radiative forcing', *Atmospheric Research*, 183: 268-82.

Li, J., H. Y. Du, Z. F. Wang, Y. L. Sun, W. Y. Yang, J. J. Li, X. Tang, and P. Q. Fu. 2017. 'Rapid formation of a severe regional winter haze episode over a mega-city cluster on the North China Plain', *Environmental Pollution*, 223: 605-15.

Li, X., Q. Zhang, Y. Zhang, L. Zhang, Y. X. Wang, Q. Q. Zhang, M. Li, Y. X. Zheng, G. N. Geng, T. J. Wallington, W. J. Han, W. Shen, and K. B. He. 2017. 'Attribution of PM2.5 exposure in Beijing-Tianjin-Hebei region to emissions: implication to control strategies', *Science Bulletin*, 62: 957-64.

Li, Y. R., C. X. Ye, J. Liu, Y. Zhu, J. X. Wang, Z. Q. Tan, W. L. Lin, L. M. Zeng, and T. Zhu. 2016. 'Observation of regional air pollutant transport between the megacity Beijing and the North China Plain', *Atmospheric Chemistry And Physics*, 16: 14265-83.

Li, Z. Q., J. P. Guo, A. J. Ding, H. Liao, J. J. Liu, Y. L. Sun, T. J. Wang, H. W. Xue, H. S. Zhang, and B. Zhu. 2017. 'Aerosol and boundary-layer interactions and impact on air quality', *National Science Review*, 4: 810-33.

Liu, Z. Q., Q. H. Liu, H. C. Lin, C. S. Schwartz, Y. H. Lee, and T. J. Wang. 2011. 'Three-dimensional variational assimilation of MODIS aerosol optical depth: Implementation and application to a dust storm over East Asia', *Journal of Geophysical Research-Atmospheres*, 116.

Lu, L. H., W. Q. Liu, T. S. Zhang, Y. H. Lu, Y. S. Dong, Z. Y. Chen, G. Q. Fan, and S. S. Qi. 2015. 'Two Data Inversion Algorithms of Aerosol Horizontal Distribution Detected by MPL and Error Analysis', *Spectroscopy and Spectral Analysis*, 35: 1774-78.

Lv, L. H., W. Q. Liu, T. S. Zhang, Z. Y. Chen, Y. S. Dong, G. Q. Fan, Y. Xiang, Y. W. Yao, N. Yang, B. L. Chu, M. Teng, and X. W. Shu. 2017a. 'Observations of particle extinction, PM2.5 mass concentration profile and flux in north China based on mobile lidar technique', *Atmospheric Environment*, 164: 360-69.

Lv, Lihui, Wenqing Liu, Tianshu Zhang, Zhenyi Chen, Yunsheng Dong, Guangqiang Fan, Yan Xiang, Yawei Yao, Nan Yang, Baolin Chu, Man Teng, and Xiaowen Shu. 2017b. 'Observations of particle extinction, PM 2.5 mass concentration profile and flux in north China based on mobile lidar technique', *Atmospheric Environment*.

Ma, C. Q., T. J. Wang, A. P. Mizzi, J. L. Anderson, B. L. Zhuang, M. Xie, and R. S. Wu. 2019. 'Multiconstituent Data Assimilation With WRF-Chem/DART: Potential for Adjusting Anthropogenic Emissions and Improving Air Quality Forecasts Over Eastern China', *Journal Of Geophysical Research-Atmospheres*, 124: 7393-412.

Ma, C. Q., T. J. Wang, Z. L. Zang, and Z. J. Li. 2018. 'Comparisons of Three-Dimensional Variational Data Assimilation and Model Output Statistics in Improving Atmospheric Chemistry Forecasts', *Advances In Atmospheric Sciences*, 35: 813-25.

Pagowski, M., Z. Liu, G. A. Grell, M. Hu, H. C. Lin, and C. S. Schwartz. 2014. 'Implementation of aerosol assimilation in Gridpoint Statistical Interpolation (v. 3.2) and WRF-Chem (v. 3.4.1)', *Geoscientific Model Development*, 7: 1621-27.

Pang, J. M., Z. Q. Liu, X. M. Wang, J. Bresch, J. M. Ban, D. Cnen, and J. Kim. 2018. 'Assimilating AOD retrievals from GOCI and VIIRS to forecast surface PM2.5 episodes over Eastern China', *Atmospheric Environment*, 179: 288-304.

Parrish, David F., and John C. Derber. 1992. 'The National Meteorological Center's Spectral Statistical-Interpolation Analysis System', *Monthly Weather Review*, 120: 1747-63.

Pokharel, Manisha, Jie Guang, Bin Liu, Shichang Kang, Yaoming Ma, Brent N. Holben, Xiang'ao Xia, Jinyuan Xin, Kirpa Ram, Dipesh Rupakheti, Xin Wan, Guangming Wu, Hemraj Bhattarai, Chuanfeng Zhao, and Zhiyuan Cong. 2019. 'Aerosol Properties Over Tibetan Plateau From a Decade of AERONET Measurements: Baseline, Types, and Influencing Factors', *Journal of Geophysical Research: Atmospheres*, 124: 13357-74.

Saide, P. E., G. R. Carmichael, Z. Liu, C. S. Schwartz, H. C. Lin, A. M. da Silva, and E. Hyer. 2013. 'Aerosol optical depth assimilation for a size-resolved sectional model: impacts of observationally constrained, multi-wavelength and fine mode retrievals on regional scale analyses and forecasts', *Atmospheric Chemistry And Physics*, 13: 10425-44.

Saide, P. E., J. Kim, C. H. Song, M. Choi, Y. F. Cheng, and G. R. Carmichael. 2014. 'Assimilation of next generation geostationary aerosol optical depth retrievals to improve air quality simulations', *Geophysical Research Letters*, 41: 9188-96.

Schwartz, C. S., Z. Q. Liu, H. C. Lin, and S. A. McKeen. 2012. 'Simultaneous three-dimensional variational assimilation of surface fine particulate matter and MODIS aerosol optical depth', *Journal Of Geophysical Research-Atmospheres*, 117.

Sheng, Z. Z., H. Z. Che, Q. L. Chen, X. A. Xia, D. Liu, Z. Z. Wang, H. J. Zhao, K. Gui, Y. Zheng, T. Z. Sun, X. P. Li, C. Liu, H. Wang, Y. Q. Wang, and X. Y. Zhang. 2019. 'Aerosol vertical distribution and optical properties of different pollution events in Beijing in autumn 2017', *Atmospheric Research*, 215: 193-207.

Su, H., Y. Cheng, and U. Poschl. 2020. 'New Multiphase Chemical Processes Influencing Atmospheric Aerosols, Air Quality, and Climate in the Anthropocene', *Acc Chem Res*.

Sun, Jinjin, Lin Huang, Hong Liao, Jingyi Li, and Jianlin Hu. 2017. 'Impacts of Regional Transport on Particulate Matter Pollution in China: a Review of Methods and Results', *Current Pollution Reports*, 3: 182-91.

Tao, W., H. Su, G. Zheng, J. Wang, C. Wei, L. Liu, N. Ma, M. Li, Q. Zhang, U. Pöschl, and Y. Cheng. 2020. 'Aerosol pH and chemical regimes of sulfate formation in aerosol water during winter haze in the North China Plain', *Atmos. Chem. Phys. Discuss.*, 2020: 1-31.

Tao, Z. M., Z. Z. Wang, S. J. Yang, H. H. Shan, X. M. Ma, H. Zhang, S. G. Zhao, D. Liu, C. B. Xie, and Y. J. Wang. 2016. 'Profiling the PM2.5 mass concentration vertical distribution in the boundary layer', *Atmospheric Measurement Techniques*, 9: 1369-76.

Tian, P. F., X. J. Cao, L. Zhang, N. X. Sun, L. Sun, T. Logan, J. S. Shi, Y. Wang, Y. M. Ji, Y. Lin, Z. W. Huang, T. Zhou, Y. Y. Shi, and R. Y. Zhang. 2017. 'Aerosol vertical distribution and optical properties over China from long-term satellite and ground-based remote sensing', *Atmospheric Chemistry And Physics*, 17: 2509-23.

Wang, J., M. Zhang, X. Bai, H. Tan, S. Li, J. Liu, R. Zhang, M. A. Wolters, X. Qin, M. Zhang, H. Lin, Y. Li, J. Li, and L. Chen. 2017. 'Large-scale transport of PM2.5 in the lower troposphere during winter cold surges in China', *Sci Rep*, 7: 13238.

Wang, L. L., J. K. Liu, Z. Q. Gao, Y. B. Li, M. Huang, S. H. Fan, X. Y. Zhang, Y. J. Yang, S. G. Miao, H. Zou, Y. L. Sun, Y. Chen, and T. Yang. 2019. 'Vertical observations of the atmospheric boundary layer structure over Beijing urban area during air pollution episodes', *Atmospheric Chemistry And Physics*, 19: 6949-67.

Wang, L. L., Z. R. Liu, Y. Sun, D. S. Ji, and Y. S. Wang. 2015. 'Long-range transport and regional sources of PM2.5 in Beijing based on long-term observations from 2005 to 2010', *Atmospheric Research*, 157: 37-48.

Wang, Y., K. N. Sartelet, M. Bocquet, and P. Chazette. 2013. 'Assimilation of ground versus lidar observations for PM10 forecasting', *Atmospheric Chemistry And Physics*, 13: 269-83.

Xiang, Y., T. S. Zhang, J. G. Liu, L. H. Lv, Y. S. Dong, and Z. Y. Chen. 2019. 'Atmosphere boundary layer height and its effect on air pollutants in Beijing during winter heavy pollution', *Atmospheric Research*, 215: 305-16.

Xiang, Yan, Lihui Lv, Wenxuan Chai, Tianshu Zhang, Jianguo Liu, and Wenqing Liu. 2020. 'Using Lidar technology to assess regional air pollution and improve estimates of PM2.5 transport in the North China Plain', *Environmental Research Letters*, 15: 094071.

Xu, J. M., L. Y. Chang, Y. H. Qu, F. X. Yan, F. Y. Wang, and Q. Y. Fu. 2016. 'The meteorological modulation on PM2.5 interannual oscillation during 2013 to 2015 in Shanghai, China', *Science of the Total Environment*, 572: 1138-49.

Yang, Xiaowen, Shuiyuan Cheng, Jianbing Li, Jianlei Lang, and Gang Wang. 2017. 'Characterization of Chemical Composition in PM2.5 in Beijing before, during, and after a Large-Scale International Event', *Aerosol and Air Quality Research*, 17: 896-907.

Yuan, R. M., X. Y. Zhang, H. Liu, Y. Gui, B. H. Shao, X. P. Tao, Y. Q. Wang, J. T. Zhong, Y. B. Li, and Z. Q. Gao. 2019. 'Aerosol vertical mass flux measurements during heavy aerosol pollution episodes at a rural site and an urban site in the Beijing area of the North China Plain', *Atmospheric Chemistry And Physics*, 19: 12857-74.

Yumimoto, K., I. Uno, N. Sugimoto, A. Shimizu, Z. Liu, and D. M. Winker. 2008. 'Adjoint inversion modeling of Asian dust emission using lidar observations', *Atmospheric Chemistry And Physics*, 8: 2869-84.

Zhang, C. X., C. Liu, K. L. Chan, Q. H. Hu, H. R. Liu, B. Li, C. Z. Xing, W. Tan, H. J. Zhou, F. Q. Si, and J. G. Liu. 2020. 'First observation of tropospheric nitrogen dioxide from the Environmental Trace Gases Monitoring Instrument onboard the GaoFen-5 satellite', *Light-Science & Applications*, 9.

Zhang, C. X., C. Liu, Q. H. Hu, Z. N. Cai, W. J. Su, C. Z. Xia, Y. Z. Zhu, S. W. Wang, and J. G. Liu. 2019. 'Satellite UV-Vis spectroscopy: implications for air quality trends and their driving forces in China during 2005-2017', *Light-Science & Applications*, 8.

Zhang, Hanyu, Shuiyuan Cheng, Sen Yao, Xiaoqi Wang, and Chuanda Wang. 2019. 'Insights into the temporal and spatial characteristics of PM2.5 transport flux across the district, city and region in the North China Plain', *Atmospheric Environment*, 218.

Zhang, Hua, Bing Xie, Shu-Yun Zhao, and Qi Chen. 2014. 'PM2.5 and tropospheric O3 in China and an analysis of the impact of pollutant emission control', *Advances in Climate Change Research*, 5: 136-41.

Zhang, Q., Y. X. Zheng, D. Tong, M. Shao, S. X. Wang, Y. H. Zhang, X. D. Xu, J. N. Wang, H. He, W. Q. Liu, Y. H. Ding, Y. Lei, J. H. Li, Z. F. Wang, X. Y. Zhang, Y. S. Wang, J. Cheng, Y. Liu, Q. R. Shi, L. Yan, G. N. Geng, C. P. Hong, M. Li, F. Liu, B. Zheng, J. J. Cao, A. J. Ding, J. Gao, Q. Y. Fu, J. T. Huo, B. X. Liu, Z. R. Liu, F. M. Yang, K.

B. He, and J. M. Hao. 2019. 'Drivers of improved PM2.5 air quality in China from 2013 to 2017', *Proceedings of the National Academy of Sciences of the United States of America*, 116: 24463-69.

Zhang, Y. H., H. Su, L. J. Zhong, Y. F. Cheng, L. M. Zeng, X. S. Wang, Y. R. Xiang, J. L. Wang, D. F. Gao, M. Shao, S. J. Fan, and S. C. Liu. 2008. 'Regional ozone pollution and observation-based approach for analyzing ozone-precursor relationship during the PRIDE-PRD2004 campaign', *Atmospheric Environment*, 42: 6203-18.

Zhang, Y. L., and F. Cao. 2015. 'Fine particulate matter (PM2.5) in China at a city level', *Scientific Reports*, 5.

Zhang, Y. X., Q. Yuan, D. Huang, S. F. Kong, J. Zhang, X. F. Wang, C. Y. Lu, Z. B. Shi, X. Y. Zhang, Y. L. Sun, Z. F. Wang, L. Y. Shao, J. H. Zhu, and W. J. Li. 2018. 'Direct Observations of Fine Primary Particles From Residential Coal Burning: Insights Into Their Morphology, Composition, and Hygroscopicity', *Journal Of Geophysical Research-Atmospheres*, 123: 12964-79.

Zhang, Y., X. Zhang, L. T. Wang, Q. Zhang, F. K. Duan, and K. B. He. 2016. 'Application of WRF/Chem over East Asia: Part I. Model evaluation and intercomparison with MM5/CMAQ', *Atmospheric Environment*, 124: 285-300.

Zhao, D., G. Liu, J. Xin, J. Quan, Y. Wang, X. Wang, L. Dai, W. Gao, G. Tang, B. Hu, Y. Ma, X. Wu, L. Wang, Z. Liu, and F. Wu. 2020. 'Haze pollution under a high atmospheric oxidization capacity in summer in Beijing: insights into formation mechanism of atmospheric physicochemical processes', *Atmos. Chem. Phys.*, 20: 4575-92.

Zheng, G. J., F. K. Duan, H. Su, Y. L. Ma, Y. Cheng, B. Zheng, Q. Zhang, T. Huang, T. Kimoto, D. Chang, U. Poschl, Y. F. Cheng, and K. B. He. 2015. 'Exploring the severe winter haze in Beijing: the impact of synoptic weather, regional transport and heterogeneous reactions', *Atmospheric Chemistry And Physics*, 15: 2969-83.

Zheng, M., C. Q. Yan, S. X. Wang, K. B. He, and Y. H. Zhang. 2017. 'Understanding PM2.5 sources in China: challenges and perspectives', *National Science Review*, 4: 801-03.

Zheng, Y., H. Z. Che, X. G. Xia, Y. Q. Wang, H. Wang, Y. F. Wu, J. Tao, H. J. Zhao, L. C. An, L. Li, K. Gui, T. Z. Sun, X. P. Li, Z. Z. Sheng, C. Liu, X. Y. Yang, Y. X. Liang, L. Zhang, C. Liu, X. Kuang, S. Luo, Y. C. You, and X. Y. Zhang. 2019. 'Five-year observation of aerosol optical properties and its radiative effects to planetary boundary layer during air pollution episodes in North China: Intercomparison of a plain site and a mountainous site in Beijing', *Science of the Total Environment*, 674: 140-58.

Zhong, J. T., X. Y. Zhang, Y. Q. Wang, J. Y. Sun, Y. M. Zhang, J. Z. Wang, K. Y. Tan, X. J. Shen, H. C. Che, L. Zhang, Z. X. Zhang, X. F. Qi, H. R. Zhao, S. X. Ren, and Y. Li. 2017. 'Relative Contributions of Boundary-Layer Meteorological Factors to the Explosive Growth of PM2.5 during the Red-Alert Heavy Pollution Episodes in Beijing in December 2016', *Journal of Meteorological Research*, 31: 809-19.

Zhou, Y. D., Y. Zhao, P. Mao, Q. Zhang, J. Zhang, L. P. Qiu, and Y. Yang. 2017. 'Development of a high-resolution emission inventory and its evaluation and application through air quality modeling for Jiangsu Province, China', *Atmospheric Chemistry and Physics*, 17: 211-33.